8-28-2018

Mannan Molecular Substructures Control Nanoscale Glucan Exposure in Candida

Matthew S. Graus
The University of New Mexico

Michael J. Wester
The University of New Mexico

Douglas W. Lowman
Quillen-Dishner College of Medicine

David L. Williams
Quillen-Dishner College of Medicine, williamd@etsu.edu

Michael D. Kruppa
Quillen-Dishner College of Medicine, kruppa@etsu.edu

See next page for additional authors

Citation Information

Graus, Matthew S.; Wester, Michael J.; Lowman, Douglas W.; Williams, David L.; Kruppa, Michael D.; Martinez, Carmen M.; Young, Jesse M.; Pappas, Harry C.; Lidke, Keith A.; and Neumann, Aaron K.. 2018. Mannan Molecular Substructures Control Nanoscale Glucan Exposure in Candida. *Cell Reports*. Vol.24(9). 2432-2442.e5. https://doi.org/10.1016/j.celrep.2018.07.088 PMID: 30157435

Mannan Molecular Substructures Control Nanoscale Glucan Exposure in Candida

Creator(s)

Matthew S. Graus, Michael J. Wester, Douglas W. Lowman, David L. Williams, Michael D. Kruppa, Carmen M. Martinez, Jesse M. Young, Harry C. Pappas, Keith A. Lidke, and Aaron K. Neumann

Article

Cell Reports

Mannan Molecular Substructures Control Nanoscale Glucan Exposure in *Candida*

Graphical Abstract

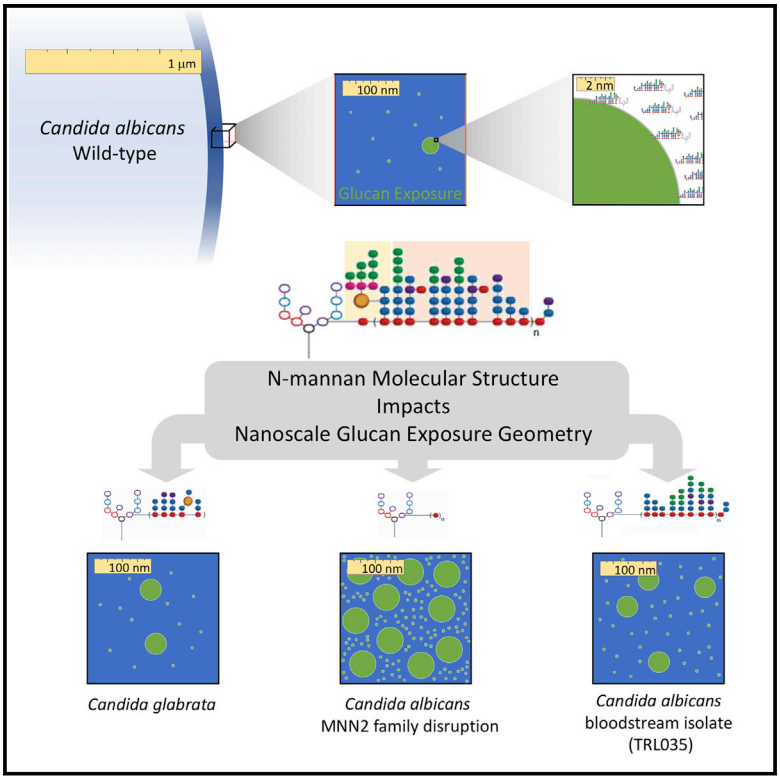

Highlights

- Immunogenic glucan exposures occur in *Candida* species pathogens at the nanoscale
- Mannosyltransferases regulate the size and density of nanoscale glucan exposures
- Elevated density and nanoscale size of glucan exposures are seen in clinical isolates

Authors

Matthew S. Graus, Michael J. Wester, Douglas W. Lowman, ..., Harry C. Pappas, Keith A. Lidke, Aaron K. Neumann

Correspondence

akneumann@salud.unm.edu

In Brief

Graus et al. find that N-mannan structural features regulated by *Candida* mannosyltransfersases control glucan exposure. Loss of mannan increased the frequency and size of glucan exposures and changed multivalent receptor engagement. Changes to mannan structure in a bloodstream isolate are associated with elevated glucan exposure at the nanoscale.

Graus et al., 2018, Cell Reports *24*, 2432–2442
August 28, 2018
https://doi.org/10.1016/j.celrep.2018.07.088

CellPress

OPEN ACCESS
CellPress

Cell Reports
Article

Mannan Molecular Substructures Control Nanoscale Glucan Exposure in *Candida*

Matthew S. Graus,[1,8] Michael J. Wester,[2] Douglas W. Lowman,[3,4] David L. Williams,[3,5] Michael D. Kruppa,[3,6] Carmen M. Martinez,[1] Jesse M. Young,[1] Harry C. Pappas,[1] Keith A. Lidke,[7] and Aaron K. Neumann[1,9,*]

[1]Department of Pathology, University of New Mexico, Albuquerque, NM 87131, USA
[2]Department of Mathematics and Statistics, University of New Mexico, Albuquerque, NM 87131, USA
[3]Center of Excellence in Inflammation, Infectious Disease and Immunity, Quillen College of Medicine, East Tennessee State University, Johnson City, TN 37684, USA
[4]AppRidge International, LLC, Telford, TN 37690, USA
[5]Department of Surgery, Quillen College of Medicine, East Tennessee State University, Johnson City, TN 37684, USA
[6]Department of Biomedical Sciences, Quillen College of Medicine, East Tennessee State University, Johnson City, TN 37684, USA
[7]Department of Physics and Astronomy, University of New Mexico, Albuquerque, NM 87131, USA
[8]Present address: European Molecular Biology Laboratory (EMBL), Australia Node in Single Molecule Science, School of Medical Sciences, University of New South Wales, Sydney, NSW 2052, Australia
[9]Lead Contact
*Correspondence: akneumann@salud.unm.edu
https://doi.org/10.1016/j.celrep.2018.07.088

SUMMARY

Cell wall mannans of *Candida albicans* mask β-(1,3)-glucan from recognition by Dectin-1, contributing to innate immune evasion. Glucan exposures are predominantly single receptor-ligand interaction sites of nanoscale dimensions. *Candida* species vary in basal glucan exposure and molecular complexity of mannans. We used super-resolution fluorescence imaging and a series of protein mannosylation mutants in *C. albicans* and *C. glabrata* to investigate the role of specific N-mannan features in regulating the nanoscale geometry of glucan exposure. Decreasing acid labile mannan abundance and α-(1,6)-mannan backbone length correlated most strongly with increased density and nanoscopic size of glucan exposures in *C. albicans* and *C. glabrata*, respectively. Additionally, a *C. albicans* clinical isolate with high glucan exposure produced similarly perturbed N-mannan structures and elevated glucan exposure geometry. Thus, acid labile mannan structure influences the nanoscale features of glucan exposure, impacting the nature of the pathogenic surface that triggers immunoreceptor engagement, aggregation, and signaling.

INTRODUCTION

The cell wall of *Candida* species yeasts is an essential feature that provides structural support and protection. There are three major polysaccharide components: mannan, β-(1,3;1,6)-glucan, and chitin (Chattaway et al., 1968). These components are organized into two layers: an inner layer primarily composed of chitin and β-glucan, and an outer layer mostly composed of cell wall proteins decorated with N- and O-linked glycosylations known as mannans (Klis et al., 2001; Netea et al., 2008; Nguyen et al., 1998; Poulain et al., 1978; Ruiz-Herrera et al., 2006). Previous evidence linking elevated glucan exposure in *Candida albicans* mutants with impaired cell wall biosynthesis has implicated N-mannan in restricting immunogenic β-glucan exposure at the cell wall surface, presumably via a steric masking effect (Wheeler et al., 2008).

N-mannans consist of an N-glycan core, an α-(1,6)-mannoside backbone, and side chains that contain α-(1,2) or (1,3) linked oligomannosides. Serotype A *C. albicans* may also possess side chain β-(1,2) or (1,3) linked oligomannosides. Additionally, acid-labile β-mannoside moieties of variable length may be appended to N-mannan side chains via phosphodiester linkages (Cutler, 2001; Hall and Gow, 2013; Hall et al., 2013; West et al., 2013). β-(1,2)- or (1,3)-linked oligomannosides have also been identified in *C. albicans* as part of the phospholipomannan moiety of the cell wall (Trinel et al., 2002). The exact structure of N-mannan varies between *Candida* species and is dependent on the expression of a complex network of mannan biosynthesis, trafficking, and cell wall remodeling genes (Shibata et al., 2012).

The outer layer of the cell wall, the point of contact between the yeast and the immune system, is predominantly composed of N-mannans with punctate exposures of β-glucan (Gantner et al., 2005). These components act as pathogen-associated molecular patterns (PAMPs), which are recognized by the immune system through pattern recognition receptors (PRRs) (Gow and Hube, 2012; Gow et al., 2011; Medzhitov and Janeway, 1997). C-type lectins (CtLs) are a class of PRRs that include DC-SIGN, mannose receptor (CD206), and Mincle, which bind to N-mannan, and Dectin-1, which binds β-glucans (Bugarcic et al., 2008; Gow et al., 2007, 2011; Netea et al., 2006; Wells et al., 2008).

Clustering is a prominent feature of PRRs and a common mechanism of regulating receptor activity (Inoue and Shinohara,

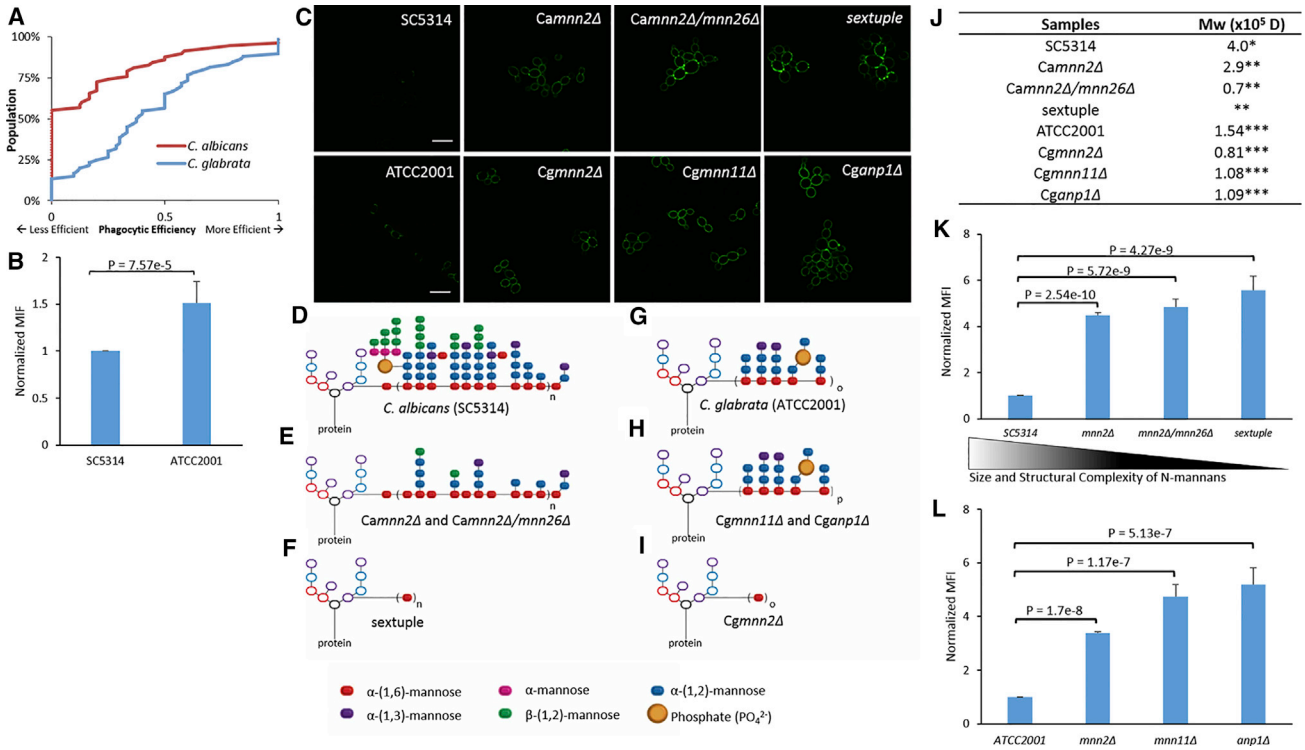

Figure 1. N-Mannan Structure Correlates with the Amount of β-Glucan Exposed

(A) Phagocytic efficiency of the distribution for populations of primary human DCs incubated with either SC5314 or ATCC2001. DCs counted, n ≥ 50.

(B, K, and L) Comparison of the integrated intensity of β-glucan measured from flow cytometry on yeasts. Statistical significance was determined by a single-tailed t test with n ≥ 20,000 gated single cells per strain. Values and error bars displayed in (B), (K), and (L) are presented as normalized medians and SDs.

(C) Representative images of yeast strains with varying amounts of β-glucan exposed. Scale bar, 10 μm.

(D–I) Schematic presentation of N-mannan structures for *C. albicans* type strain (SC5314) (D), *Camnn2*Δ and *Camnn2*Δ/*mnn26*Δ (E), *C. albicans* MNN2 family sextuple mutant (F), *C. glabrata* type strain (ATCC2001), Cg*mnn11*Δ and Cg*anp1*Δ (H), and Cg*mnn2*Δ (I). Subscripts n, o, and p correspond to an unspecified number of repeats > 1, and o > p. Structures in (E) and (F) structures are recreated similarly to those depicted in Hall et al. (2013). Structures in (G)–(I) are recreated similarly to those depicted in West et al. (2013).

(J) Molecular weights of type strains and mannosylation mutants. *Data from Kruppa et al. (2011). **Data from Hall et al. (2013); sextuple data were not available. ***Data from West et al. (2013).

2014). Previously, we reported changes in CtL nanocluster geometry during fungal particle recognition and the presence of nanoscale ligand patterns on *C. albicans* cell walls (Itano et al., 2012; Lin et al., 2016). We have also reported that *C. albicans* glucan is sparsely accessible on lateral yeast and hyphal cell walls, consisting of single glucan/Dectin-1 interaction sites as well as larger (~40 nm diameter) exposures (Lin et al., 2016). Recent studies on reactive oxygen species (ROS) generation from glucan-coated particles of varying size (50, 200, or 500 nm diameter) (Goodridge et al., 2011) suggest that ligand presentation geometry may influence Dectin-1 clustering and signaling. Multimerization of Dectin-1 upon ligand engagement is thought to be important for signal transduction via the receptor's hemITAM domains. Therefore, the nanoscale geometry of glucan exposure is likely to impact Dectin-1 signaling and generation of innate immune anti-fungal responses.

In this report, we sought to better define nanometric glucan exposure geometries by determining structural features of *C. albicans* and *C. glabrata* N-mannans that regulate glucan exposure geometry at the molecular level.

RESULTS

Phagocytic Response and β-Glucan Exposure Varies between Species

We began the study by measuring phagocytosis efficiencies between *C. albicans* (SC5314) and *C. glabrata* (ATCC2001) on dendritic cells (DCs). DCs co-cultured with ATCC2001 had a higher phagocytic efficiency than DCs co-cultured with SC5314 (Figure 1A).

Glucan exposure has been linked to phagocytosis in other studies (Graus et al., 2014; Hardison and Brown, 2012), suggesting that differences in the amount of glucan exposed could relate to the changes in phagocytic efficiencies. Although the *C. albicans* cell wall contains 10% more β-glucan and 17% less mannose than *C. glabrata* (de Groot et al., 2008) by dry mass, flow cytometry determined that β-glucan exposure was 1.5-fold greater on *C. glabrata* than on *C. albicans* (Figures 1B and 1C). This suggests that glucan exposure and DC phagocytic uptake are not necessarily correlated with cell wall glucan abundance and led to the hypothesis that the molecular structure of

mannan may be the major determinant of glucan exposure. Consistent with this hypothesis, previous studies reported the molecular weight of *C. albicans* N-mannans to be 2.6-fold greater than that of *C. glabrata* (Hall et al., 2013; West et al., 2013). In addition, the molecular structure of *C. glabrata* mannan is lower in structural complexity relative to *C. albicans* (Shibata et al., 2012).

Comparison of N-Mannan Structure in *C. albicans* and *C. glabrata* Strains

Gene deletion mutants that have significant and known defects in mannan biosynthesis were used to explore the possibility that size and molecular complexity of N-mannans determines the ability of those mannans to sterically hinder access of receptors to glucan, thus regulating surface glucan exposure. We began with the CaMNN2 gene family mannosylation mutants previously characterized by Hall et al. (2013). This gene family is responsible for normal abundance and complexity of N-mannan side chains (Hall et al., 2013; Rayner and Munro, 1998), and deletion mutant strains of the CaMNN2 family exhibit altered mannan structure. The *C. albicans* parental strain was compared to the mannosylation mutants *mnn2*Δ, *mnn2*Δ/*mnn26*Δ, and a sextuple mutant (all CaMNN2 gene family deleted). In general, as the number of CaMNN2 genes deleted increased, the molecular weight and structural complexity of the mannans declined, but because of the higher multiplicity of MNN2 family members in *C. albicans*, a greater variety of mannan structures are produced relative to *C. glabrata*, wherein only one MNN2 gene has been characterized. Specifically, Ca*mnn2*Δ and Ca*mnn2*Δ/*mnn26*Δ were previously found to be structurally similar by NMR with regard to the types of side chain structures present and lacking. CaMMN2 family mutant strains exhibited marked reduction in acid-labile mannan fraction and reduced abundance and complexity of side chains relative to the parental strain, along with diminishing molecular weight as the severity of mutation increased (Figures 1D, 1E, and 1J). The *C. albicans* sextuple MNN2 family deletion mutant produces the most severely perturbed mannan, containing only a unsubstituted α-(1,6)-mannose backbone. This makes the sextuple mutant's mannan most structurally analogous to the Cg*mnn2Δ* mannan investigated below (Figures 1F and 1I). There is no direct analog between Ca*mnn2*Δ and Ca*mnn2*Δ/*mnn26*Δ mutant's mannans and the *C. glabrata* mannans investigated below as a result of their more extensive side-chain defects and more extreme diminution of molecular weight. Based on previous work (Hall et al., 2013), we hypothesized that the negatively charged acid labile mannan as well as the large complex side chains are important N-mannan features for regulating nanoscale features of β-glucan exposure.

Analysis of Glucan Exposure in *C. albicans* Strains

Measurement by flow cytometry of the *C. albicans* mannosylation mutants showed that total glucan exposure increased as N-mannan size and structural complexity decreased, resulting in a 4.5- to 5.5-fold increase in total exposure relative to SC5314 (Figures 1C and 1K).

Processes that unmask glucan change not only the total amount of glucan exposed, but also the nanostructural features of glucan presentation to innate immunoreceptors like Dectin-1 (Lin et al., 2016). Direct stochastic optical reconstruction microscopy (dSTORM) was used to explore the unmasking process. dSTORM data were quantified with the hierarchical single emitter hypothesis test (H-SET) and two different clustering algorithms to measure the geometry and characteristics of the exposures. H-SET is able to correct common artifacts in dSTORM imaging arising from multiple localizations of individual probes, allowing accurate structural representation of nanoscale objects (Lin et al., 2016). The clustering algorithms, hierarchical-based clustering, and Voronoï tessellation-based segmentation (Levet et al., 2015) define clusters and measure nanoscopic cluster characteristics.

dSTORM imaging revealed that the majority of exposures in all strains are single-probe binding events with the sextuple mannosylation mutant having the highest density of single-probe events (Figures 2A–2D and S1A–S1C). When compared to SC5314, all mannosylation mutants possess significantly more glucan multi-exposures that are larger in diameter (Figures 2E, 2F, S1D, and S1E). In the most severely affected sextuple mutant, glucan exposure density increased by 4.5-fold (relative to SC5314) and median exposure radius increased from 14 nm (SC5314) to 21 nm (sextuple mutant). We conclude that N-mannan side-chain feature deficiencies affect glucan unmasking by increasing both the number of exposures on the cell wall and the sizes of the exposures. The side-chain characteristics altered in these mutant strains appear to control glucan exposure nanostructure through diminished density of side chains and the loss of acid-labile mannan.

Analysis of Glucan Exposure in *C. glabrata* Strains

To study how N-mannan structure affects glucan exposure in the relatively small mannans of *C. glabrata*, mannosylation mutants from West et al. (2013) were utilized. The authors demonstrated alterations in mannan structure of Cg*anp1Δ*, Cg*mnn11Δ*, and Cg*mnn2Δ* relative to the parental strain, ATCC2001. N-mannans in the mannosylation mutants are smaller than that of the parental strain, with Cg*mnn2Δ* mannan having the largest decrease in molecular weight (West et al., 2013) (Figure 1J). Both Cg*anp1Δ* and Cg*mnn11Δ* strains have a reduced length of the mannan α-(1,6)-mannose backbone but retain the α-(1,2) and α-(1,3)-mannose side chains in reduced abundance because of the shorter backbone (Figure 1H). Cg*mnn2Δ* mannan has an unsubstituted α-(1,6)-mannose backbone similar to the sextuple mutant (Figures 1F and 1I). Furthermore, Cg*mnn11Δ* and Cg*anp1Δ* retain the acid-labile fraction of its mannan, but this negatively charged constituent is missing in Cg*mnn2Δ*. We hypothesized Cg*mnn2*Δ would have the largest amount of β-glucan exposed due to the lack of space-filling side chains that are likely be important for steric masking of underlying glucan.

All three mannosylation mutants exhibit increased amounts of glucan exposed relative to the parental *C. glabrata* strain. Surprisingly, Cg*mnn2Δ* exhibited the smallest increase in glucan exposure, while Cg*mnn11Δ* and Cg*anp1Δ* had much larger increases in comparison to ATCC2001 with fold increases that ranged from 3.3 to 5 (Figures 1C and 1L). The reduction of the α-(1,6)-mannose backbone length in Cg*mnn11Δ* and Cg*anp1Δ* unexpectedly plays a more significant role on N-mannan's ability to mask glucan efficiently. To understand how the shortening of the

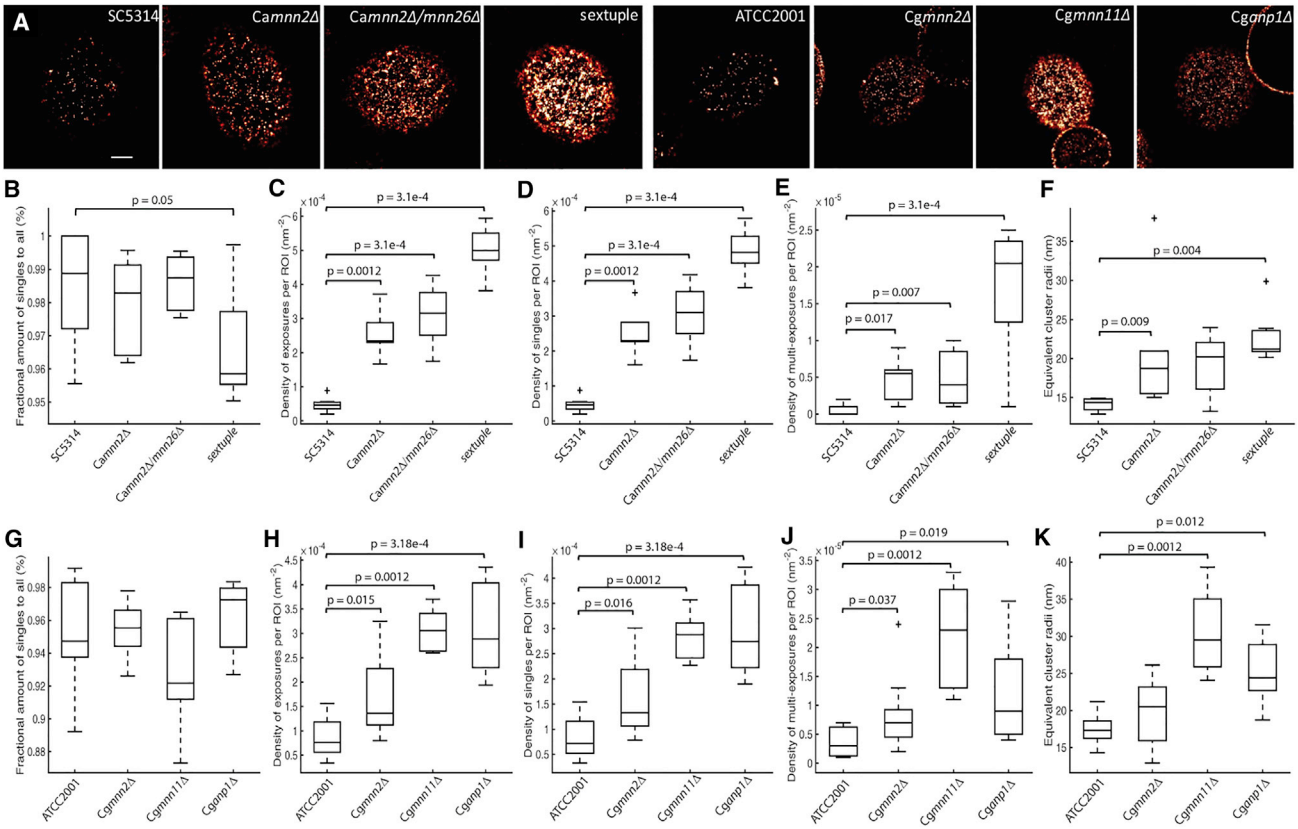

Figure 2. Nanoscopic β-Glucan Exposure Characteristics Are Determined by N-Mannan Structure

(A) Representative dSTORM images of type strains and mannosylation mutants. Scale bar, 750 nm.

(B–F) Hierarchical clustering quantification of nanoscopic glucan exposure geometries on *C. albicans* strains for a fractional amount of singlet glucan exposures relative to all glucan exposures (B), density of exposures (C), density of singlet exposures (D), density of multi-exposures (E), and equivalent glucan exposure radii (F).

(G–K) Hierarchical clustering quantification of nanoscopic glucan exposure geometries on *C. glabrata* strains for a fractional amount of singlet glucan exposures relative to all glucan exposures (G), density of exposures (H), density of singlet exposures (I), density of multi-exposures (J), and equivalent glucan exposure radii (K). Boxplots represent population of events found in each ROI. Statistical significance was determined by Mann-Whitney *U* test with $n \geq 6$ cells for each strain. See also Figures S1, S4, and S5.

α-(1,6)-mannose backbone affects unmasking, dSTORM imaging was used to examine the *C. glabrata* mannosylation mutants.

Similar to the *C. albicans* mannosylation mutants, the majority of exposures identified in the *C. glabrata* dataset are single-probe binding events (Figures 2A, 2G–2I, and S1F–S1H). Interestingly, shortening of the α-(1,6)-mannose backbone has the greatest effect on increasing the density of nanoscale glucan exposures, with a 1.5-fold increase in clustered glucan exposures for *Cgmnn2Δ* relative to ATCC2001, and the median exposure size increases from 21 nm (*Cgmnn2Δ*) to 29 nm (*Cgmnn11Δ*). The data suggest that the ability to extend a side-chain-decorated mannan backbone in space is the most critical parameter for overall glucan masking and the density of glucan nanoexposures in *C. glabrata*.

Analysis of Glucan Exposure in *Candida* Clinical Isolate Strains

We extended the study by investigating glucan exposure in recent clinical isolates of *C. albicans* and *C. glabrata*. Most *C. albicans* and *C. glabrata* clinical isolates have low levels of glucan exposure, similar to the SC5314 and ATCC2001 type strains (Figure S2A; data not shown). However, one *C. albicans* isolate (TRL035) and one *C. glabrata* isolate (TRL031) were found that exhibited a total glucan exposure 3.1-fold greater than SC5314 and 1.5-fold greater than ATCC2001, respectively (Figures S2A–S2D).

Due to its unusual cell wall phenotype, TRL035's identity was confirmed as *C. albicans* by several methods. In sum, classification of this isolate as *C. albicans* was supported by positive results from mass spectrometric identification with a score of 2.19 (Bruker Biotyper, Tricore Reference Laboratories), fungal ribosomal DNA ITS2 sequencing (Charles River Laboratories, Accugenix FunITS), growth on chromagar, and filamentation assays. Similar assays were also completed for TRL031, confirming its identification as *C. glabrata*.

As a result of the marked increase in overall glucan exposure of both isolates, we hypothesized that the N-mannan in both samples must be deficient in specific features and would result in nanoscale alterations of glucan exposure sites similar to the mannosylation mutant strains described above. dSTORM

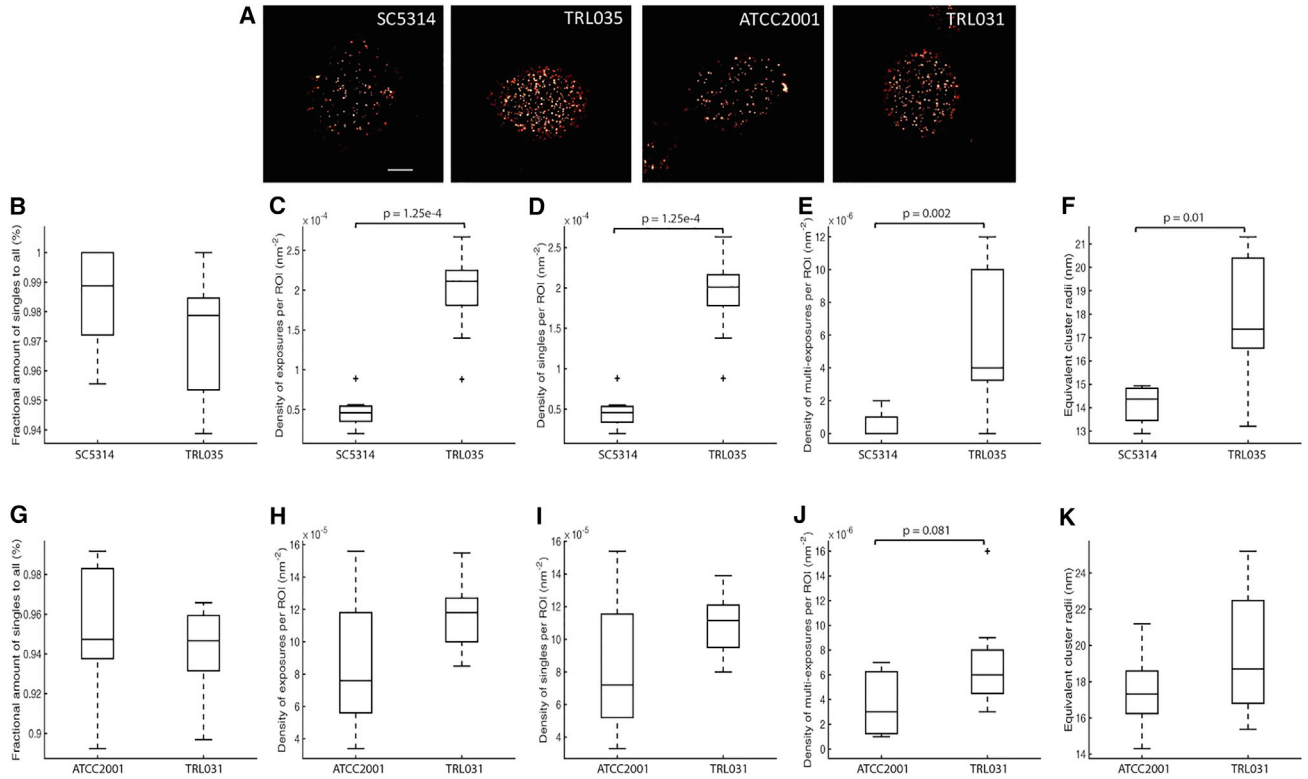

Figure 3. Clinical Isolates Nanoscopic β-Glucan Exposure Characteristics Are Dissimilar from Type Strains

(A) Representative dSTORM images of type strains and clinical isolates. Scale bar, 750 nm.

(B–F) Hierarchical clustering quantification of nanoscopic glucan exposure geometries on *C. albicans* strains for a fractional amount of singlet glucan exposures relative to all glucan exposures (B), density of exposures (C), density of singlet exposures (D), density of multi-exposures (E), and equivalent glucan exposure radii (F).

(G–K) Hierarchical clustering quantification of nanoscopic glucan exposure geometries on *C. glabrata* strains for a fractional amount of singlet glucan exposures relative to all glucan exposures (G), density of exposures (H), density of singlet exposures (I), density of multi-exposures (J), and equivalent glucan exposure radii (K). Boxplots represent population of events found in each ROI. Statistical significance was determined by Mann-Whitney *U* test with $n \geq 6$ cells for each strain. See also Figures S2–S5.

imaging of TRL035 confirmed that the density of both single-probe binding events and multi-exposures significantly increased, and there was a significant increase in the median size of the exposures (Figures 3A–3F and S3A–S3E). The increase in both density and size of exposures mirrors what was observed in the *C. albicans* mannosylation mutants, specifically in the C*amnn2Δ* mutant, leading us to hypothesize that TRL035's N-mannan is deficient in some side-chain features, along with the acid-labile fraction.

dSTORM imaging revealed that glucan multi-exposure density was slightly higher in TRL031 relative to ATCC2001 (Figures 3J and S3I). No other nanoscale glucan exposure features were regarded to be significantly different (Figures 3A, 3G–3K and S3F–S3J). When compared, the nanoscale exposure characteristics of TRL031 closely resembles the C*gmnn2Δ* mutant, leading to the hypothesis that TRL031s' N-mannan is moderately deficient in side chains and acid-labile features.

Physicochemical and Structural Analysis of N-Mannan from *Candida* Clinical Isolates

To test if TRL035 and TRL031 have similar N-mannan features as the type strains, gel permeation chromatography (GPC) with multiangle laser light scattering detection (MALLS) and ^{1}H NMR were performed to determine the structure of the mannans. Mannan extraction was done on both isolates using an alkali bath method modified from Li et al. (2009). TRL031's mannoprotein molecular weight was found to be very similar to ATCC2001's (Figures 1J and 4A). Poor yield of TRL035 mannoprotein, most likely due to small size, necessitated an alternate mild alkali extraction method. TRL035's mannoproteins were ~3-fold smaller than previously reported values for SC5314 (Figures 1J and 4A). Pronase treatment of TRL035 mannoprotein led to lower-molecular-weight mannan (66% decrease in molecular weight) and a narrower polydispersity of mannans (Figure 4A). In summary, GPC analysis shows that clinical isolate strain TRL035 produces significantly smaller N-mannans than type strain and is completely lacking high-molecular-weight mannoproteins characteristically found in *C. albicans*, whereas TRL031 produces similarly sized mannoproteins as characteristically found in *C. glabrata*.

We considered that the reduction in mannan size in TRL035 was likely because of lower structural complexity of the mannan. To confirm this hypothesis, ^{1}H NMR was used for analysis of TRL035 mannan structure. TRL035 has major resonances in

A

Sample	Mw (x10^5 Da)	%Δ	Polydispersity (Mn/Mw)	Mark-Houwink (α)
TRL031	1.3	---	1.39	0.51
TRL035	1.3	---	2.26	0.44
TRL031 + Pronase	0.77	-39.1	1.25	1.63
TRL035 + Pronase	0.46	-66.1	1.55	**

B

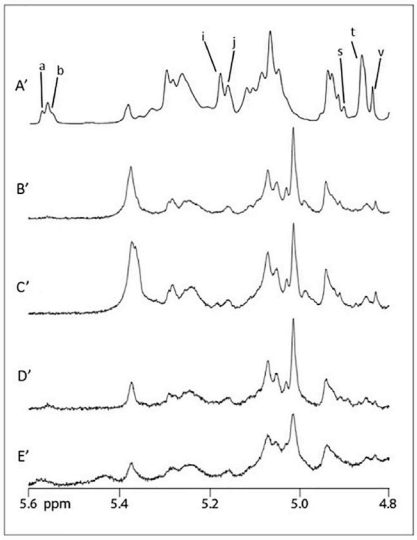

C

Label	H1	Assignment
a	5.568*	β-M-(1→2)-α-**M**-(1→PO_4
b	5.556*	β-M-(1→2)-[β-M-(1→2)]$_n$-β-M-(1→2)-α-**M**-(1→PO_4
	5.280	Mβ1-2**M**α1-3
	5.244	Mα1-2(Mα1-2)$_n$**M**α1-2
	5.237	Mβ1-2(Mβ1-2)$_n$**M**α1-3
	5.160	Mβ1-2Mβ1-2**M**α1-3
	5.158	Mα1-3
	5.068	-6(Mα1-2)Mα1-6(**M**α1-2Mα1-2)Mα1-
	5.050	α1-3**M**α1-2
	5.002	Mβ1-2**M**β1-2Mβ1-2Mβ1-2Mα1-2
	4.933	Related to **M**α1-6 ?
	4.927	Mβ1-2Mβ1-2Mβ1-2Mβ1-2Mα1-2
	4.832	Mβ1-2Mβ1-2
i	5.183*	β-M-(1→2)-α-**M**-(1→2)
j	5.163*	β-M-(1→2)-α-**M**-(1→2)
s	4.902*	β-M-(1→2)-[β-M-(1→2)]$_n$-β-**M**-(1→2)-α-M-(1→PO_4
t	4.855*	β-M-(1→2)-β-**M**-(1→2)-α-M-(1→2(3))
t	4.853*	β-M-(1→2)-β-**M**-(1→2)-α-M-(1→PO_4
u	4.832*	β-**M**-(1→2)-α-M-(1→PO_4

D

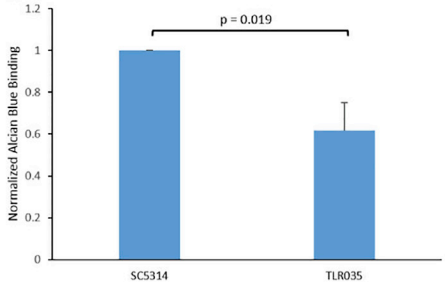

E

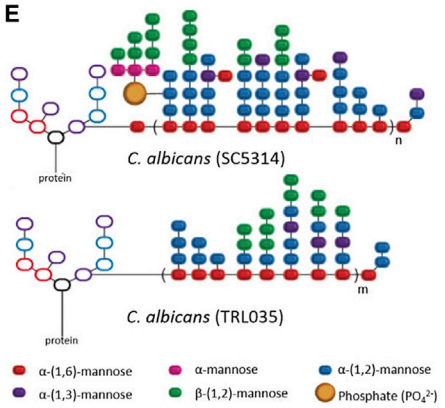

Figure 4. Physicochemical Analysis Shows Loss of the Acid-Labile Fraction in TRL035 N-Mannan

(A) GPC analysis of TRL031 and TRL035. Asterisks (**) denote samples from which data could not be obtained due to low sample yield.

(B and C) NMR analysis of TRL035.

(B) Stacked spectral plot comparing SC5314 (A′), TRL035 (B′ and D′), and TRL035 pronase treatment (C′ and E′). (B′), (C′), (D′), and (E′) are from different cell wall isolations.

(C) Table of structural motif assignments for mannan. ^{1}H chemical shifts with an asterisk are taken from Lowman et al. (2011) to show where acid-labile resonances are present in (A′).

(D) Comparison of the amount of Alcian blue bound per yeast. Statistical significance was determined by a single-tailed t test with an n = 3. Values and error bars displayed are presented as normalized means and SDs.

(E) Proposed N-mannan structure of TRL035 (bottom) based on NMR analysis compared to SC5314 (top). Subscripts n and m correspond to an unspecified number of structural repeats > 1, and n > m. The structure of mannan from SC5314 (top) is recreated similarly to that depicted in Hall et al. (2013).

the carbohydrate spectral region from 3.3 to 5.6 ppm, some of which provide information on mannan side-chain structure. TRL035 mannan almost completely lacks the acid labile mannan resonances found abundantly in SC5314 mannan at 5.568, 5.183, 4.902, 4.855, 4.853, and 4.832 ppm (Figures 4B and 4C). Loss of the acid-labile mannan, containing a phosphodiester linkage, is anticipated to decrease the negative charge of the cell wall surface, which results in reduced binding of the polycationic dye Alcian blue. Confirmation of TRL035 acid-labile mannan deficiency was observed by the reduced Alcian blue staining for TRL035 versus SC5314 (Figure 4D). Because TRL035 has a clear deficiency in the acid-labile fraction, existing side-chain resonances are assigned to the acid-stable mannan fraction. TRL035 mannan's signal at 5.068 ppm indicates, as expected, the presence of substituted α-(1,6)-linked backbone residues. Furthermore, the lack of a signal at 5.117 ppm for unsubstituted α-(1,6)-mannose suggests that the TRL035 mannan does not possess interspersed regions of acid-stable side-chain-free backbone (e.g., as was observed in C*amnn2*Δ, C*amnn2*Δ/*mnn26*Δ, and C*amnn2* family sextuple mutant strains). The acid-stable side chains are shown to be terminated in both α- and β-mannose units by the presence of signals at 5.280 ppm, 5.244 ppm, and 5.002 ppm (Figures 4B and 4C). Based on the NMR resonances found above, we constructed the most likely N-mannan structure for TLR035 (Figure 4E).

Similar to TRL035, we also performed ^{1}H NMR on TRL031. Compared to ATCC2001, TRL031 mannan lacks the resonances for the acid-labile fraction of the mannan found in ATCC2001 at 5.555, 5.754, and 4.855 ppm (Figures 5A and 5B). The Alcian blue assay was attempted to confirm loss of acid-labile fraction on TRL031 at the above chemical shifts (Figure 5C). However, acid-labile mannan is much less abundant in ATCC2001 than SC5314, making its loss in TRL031 a mild phenotype that was undetectable by the Alcian blue assay. Acid-stable resonances in ATCC2001 are also present in TRL031, showing that no additional loss of N-mannan features has occurred (Figure 5D). TRL031 shows some similarities to the C*gmnn2Δ* mutant in that both strains have increased total glucan exposure along with increased size and density of the exposures that correlate with the loss of the acid-labile fraction of the N-mannan.

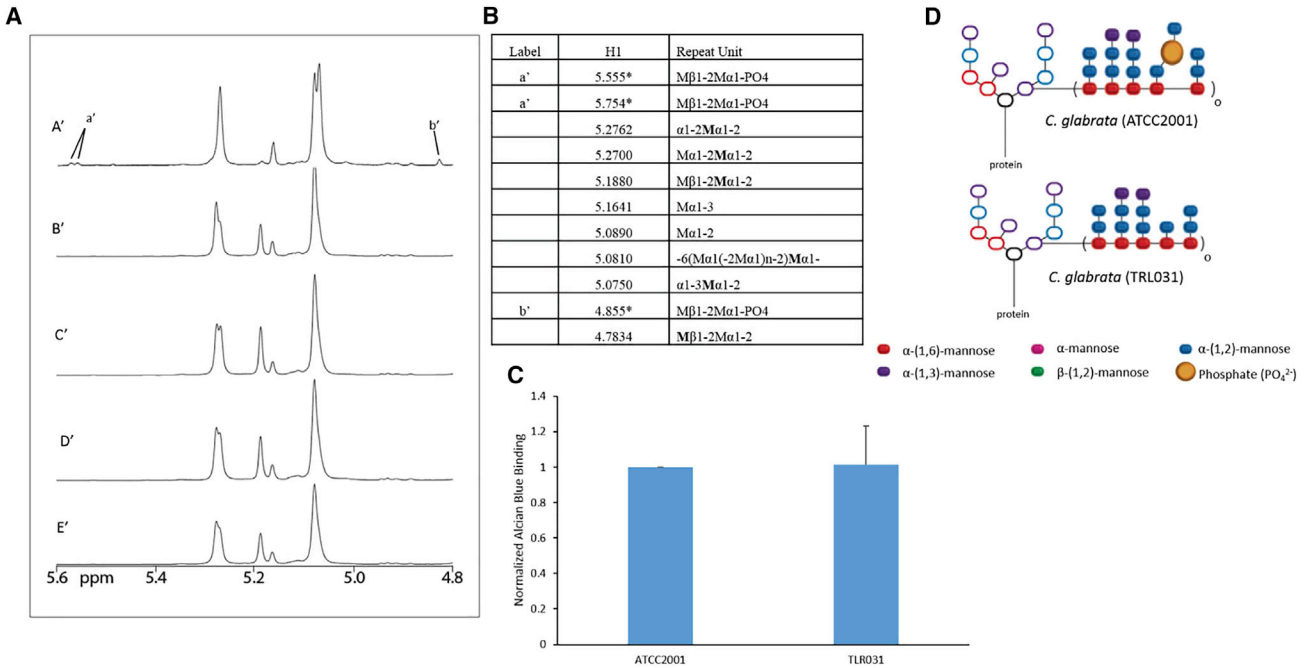

Figure 5. Physicochemical Analysis Shows Loss of Acid Labile Fraction in TRL031 N-Mannan

(A) Stacked spectral plots comparing ATCC2001 (A′), TRL031 (B′ and D′), and TRL031 pronase treatment (C′ and E′). B′, C′ and D′, E′ are from different cell wall isolations.

(B) Table of structural motif assignments for mannan. ^{1}H chemical shifts with an asterisk are taken from West et al. (2013) to show where missing acid-labile resonances are present in A′.

(C) Comparison of the amount of Alcian blue bound per yeast. Statistical significance was determined by a single-tailed t test with an n = 3 biological replicates. Values and error bars displayed are presented as normalized means and SDs.

(D) Proposed N-mannan structure of TRL031 based on NMR analysis compared to ATCC2001. Subscript o denotes an unspecified number of structural repeats > 1.

Taken together, the GPC and NMR data reveal an N-mannan structure in TRL035 that bears some similarities to *C. albicans* mannosylation mutant strains. More specifically, the loss of the acid-labile fraction, which provides not only bulk but also negative charge, in *C. albicans* mannan is a feature that correlates with increased total glucan exposure as well as the size and density of nanoscale glucan exposure sites. The existence of clinical isolate strains that have acquired a mannan structure with high glucan exposure further indicates that regulation of glucan exposure through manipulation of mannan structure is not limited to artificial mutations but can also be a part of the disease process in patients with candidiasis.

DISCUSSION

The outer layer of the yeast cell wall plays an essential role in protection and immune evasion. It is thought that the N-mannans of the yeast cell wall play a pivotal role in hindering Dectin-1 from binding to β-glucan. In this report, we define how specific N-mannan structural features affect immune evasion through the alteration of glucan exposure geometries at the molecular level. Our findings strongly implicate N-mannan side-chain abundance and complexity in *C. albicans* and backbone length in *C. glabrata* as features that are important for masking glucan. In *C. albicans*, we found that as little as a single deletion in the MNN2 gene family can increase glucan exposure by over 4-fold (Figures 1K and 2B). This could result from the loss of the negatively charged acid-labile mannan, leading to less efficient glucan masking. Increasing the number of MNN2 gene family deletions increased the degree to which nanoscale glucan exposure phenotype changed. Among the *C. glabrata* mutants, the most significant changes to glucan exposure size and density arose from the mutants that have shortened backbones (Cg*mnn11Δ* and Cg*anp1Δ*). Consistent with this, Cg*mnn2Δ*, which has the lowest-molecular-weight N-mannans of the *C. glabrata* mutant series and only an unsubstituted mannan backbone, was able to provide glucan masking better than Cg*mnn11Δ* and Cg*anp1Δ,* which do retain some acid-stable side-chain structure.

Mannan masking of glucan in the cell wall can play a significant role in recognition of *C. albicans* and *C. glabrata* by the immune system. We showed that the ATCC2001 type strain of *C. glabrata* exhibits higher glucan exposure and more efficient phagocytic uptake by human-monocyte-derived DCs than *C. albicans* (SC5314). Deletion of MNN2 family members is associated with increased glucan exposure in both *C. albicans* and *C. glabrata*. It is notable that previous studies have shown that these *C. albicans* MNN2 family mutants are hypovirulent in infection models, but the *C. glabrata* MNN2 mutants are hypervirulent (Hall et al., 2013; Rouabhia et al., 2005; West et al., 2013). Why does glucan exposure decrease virulence in *C. albicans* but

increase virulence in *C. glabrata*? Hypovirulence of MNN2 family mutants in *C. albicans* may be explained with reference to enhanced host defense due to greater stimulation of glucan receptors such as Dectin-1 and CR3. On the other hand, *C. glabrata* has been shown to be able to survive and replicate within phagosomes (Seider et al., 2011), so more efficient entry into the phagosomal environment may promote survival, dissemination, and evasion of immune detection for this pathogen, as discussed in greater detail below.

Previous physicochemical studies of *C. albicans* sextuple and *C. glabrata mnn2*Δ mutants have revealed that N-mannans from these strains are both composed of a largely unsubstituted α-(1,6)-mannan chain (Hall et al., 2013; West et al., 2013). Interestingly, dSTORM analysis of glucan exposure densities and size indicated that *C. albicans* sextuple mutant had larger total, singlet, and multi-exposure glucan exposure density and somewhat larger glucan multi-exposure size relative to *C. glabrata mnn2*Δ mutant. Prior studies have obtained a molecular weight of *C. glabrata mnn2*Δ mutant mannan, but *C. albicans* sextuple mutant mannan has proven exceedingly difficult to extract, most likely due to its very small size. Therefore, the molecular weight distribution of *C. albicans* sextuple mutant mannan is currently unknown, and we were unable to overcome this limitation in our study. Nevertheless, the extractability of *C. glabrata mnn2*Δ mutant mannan, but not *C. albicans* sextuple mutant mannan, suggests that the overall size of *C. albicans* sextuple mutant mannan may be even smaller than of *C. glabrata mnn2*Δ mutant mannan. It is tempting to speculate that smaller *C. albicans* sextuple mutant mannan may provide even poorer glucan masking than *C. glabrata mnn2*Δ mutant mannan, leading to the stronger glucan exposure phenotype in the *C. albicans* sextuple mutant.

Extending our work to patient samples, we found two clinical isolates with unusually high glucan exposures, TRL035 and TRL031. It is not yet clear how TRL035 acquired its high glucan exposure phenotype. It is possible that perturbation of one or more MNN2 family genes play a role, but other gene deletions cause increased glucan exposure. *cho1*Δ, *cek1*Δ, and *kre5*Δ strains exhibit increased glucan exposure and Dectin-1 binding (Davis et al., 2014; Galán-Díez et al., 2010; Herrero et al., 2004; Wheeler and Fink, 2006). *goa1*Δ mutants have recently been shown to have reductions in both β-(1,2)-linked mannose units and acid-labile mannan (She et al., 2016), which bears some similarity to the TRL035 mannan phenotype. Future work will pursue molecular mechanistic explanations of mannan biosynthesis, glucan exposure, and the pathological states associated with this and other high-glucan clinical *Candida* isolate strains.

The cause of high glucan exposure in TRL031 is also unclear. None of the *C. glabrata* mutants we investigated are structurally similar to TRL031. Based on GPC and NMR analysis, TRL031 does not seem to have a shortening of its α-(1,6)-mannose backbone or a loss of side chains. The only difference detected in the N-mannan structure is the loss of the acid-labile fraction, suggesting that the negatively charged fraction of the N-mannan plays a role in glucan masking. More research on mannosylation mutants is required to fully understand the effects of N-mannan biosynthesis on glucan exposure.

We consistently saw correlation of loss of acid-labile mannan structure with increases in total glucan exposure and both the size and density of nanoscale glucan exposure features. It is therefore tempting to speculate that acid-labile mannan is at least one important regulator of glucan exposure nanostructure. Deletion of the CaMNN4 gene is associated with a more specific loss of acid-labile mannan structure. Past reports have varied with respect to the impact of this defect on innate immune recognition of *C. albicans*. Hobson et al. examined a Ca*mnn4*Δ strain and reported no defect in virulence or phagocytic uptake at high yeast/phagocyte ratios (Hobson et al., 2004). However, McKenzie et al. (2010) did find that phagocytosis of a Ca*mnn4*Δ strain was significantly different from yeast with wild-type mannan. Furthermore, Ueno et al. (2013) found that purified mannan from a Ca*mnn4*Δ strain induced significantly lower interleukin-6 (IL-6) and IL-12p40 responses *in vitro* relative to wild-type mannan. These studies suggest that acid-labile mannan structure may be an important factor in host-pathogen interactions during *Candida* species recognition by leukocytes. Our work suggests that future investigations into the role of CaMNN4 on glucan exposure on the micro- and nanoscale are indicated to further clarify the role of acid-labile mannan in glucan masking.

Increased chitin exposure, often in concert with glucan exposure, has been reported in *C. albicans* and *A. fumigatus* after neutrophil attack, in low-pH conditions, and after echinocandin exposure (Amarsaikhan et al., 2017; Hopke et al., 2016; Sherrington et al., 2017; Wheeler and Fink, 2006). These may represent coordinate responses to cell wall stress signaling. It is possible that increased chitin deposition and exposure in the outer cell wall might lower the density of glucan, specifically β-(1,6)-glucan attachment points for mannoproteins, thus decreasing glucan masking. Finally, chitin exposure can trigger anti-inflammatory cytokine responses and arginase expression (Elieh Ali Komi et al., 2018; Mora-Montes et al., 2011; Wagener et al., 2017), suggesting that innate immune responses to *Candida* cell walls may be variously impacted by glucan and chitin levels present at their surfaces.

To determine whether chitin was altered in the strains used in this study, we assessed chitin content (calcofluor white) and exposure (wheat germ agglutinin) by flow cytometry (Figure S4). We confirmed the previous observation that the *C. albicans* MNN2 family mutants used in this study exhibited increases in chitin content and exposure, most notably for sextuple mutant (Hall et al., 2013). TRL035 chitin content and exposure were only mildly increased (less than 2-fold) relative to type strain. In contrast, the increase in glucan exposure we observed in TRL035 was much stronger. Chitin and glucan exposure responses may reflect coordinate cell wall remodeling responses in this isolate strain, and both polysaccharides are likely to influence the response to this and other *Candida* species pathogens. *C. glabrata* mutants used in this study exhibited increases in chitin deposition and exposure, most strongly for Cg*anp1*Δ. However, clinical isolate *C. glabrata* strain TRL031 did not have significant increase in chitin. It is possible that *C. glabrata* and *C. albicans* mask glucan in different ways or that the ability to control glucan exposure is more important for *C. albicans* than *C. glabrata*. We found that *C. glabrata* had increased glucan exposure (Figures 1A and 1B) and was phagocytosed more readily. *C. glabrata* is known to be resistant to phagolysosomal killing (Kaur et al., 2007; Roetzer et al., 2010; Seider et al.,

2011) and can replicate intracellularly. Indeed, it has been proposed that *C. glabrata* is adapted to utilize phagosomal compartments as a protective host niche (Kasper et al., 2015). Therefore, glucan masking may be less critical in this pathogen and may even promote access to an advantageous intracellular niche. However, the role of mannan structure is likely to be complex, as *C. glabrata* mannosyltransferase mutants display defects in phagosomal alkalization and survival (Kasper et al., 2014), suggesting roles for protein mannosylation that may extend beyond their contribution to glucan masking.

Understanding the regulation of nanoscale glucan features by mannan structure is necessary for a more complete mechanistic appreciation of early events in pathogen recognition by innate immune cells. Dectin-1 signaling via its cytoplasmic hemITAM motif is thought to require ligand-dependent multimerization of the receptor (Inoue and Shinohara, 2014). The majority of glucan exposure sites on *C. albicans* cell walls are single receptor-ligand interaction sites (Lin et al., 2016) that may not support Dectin-1 multimerization. However, we have shown that exposure sites large enough for multimerization exist, which are composed of clusters of multiple exposed glucan-binding sites. We have also shown that perturbed mannan structures result in an increase in the surface density and individual size of these exposures. It is likely that these more complex exposed glucan nanostructures play critical roles in determining the multimerization of Dectin-1 and initiating innate immune responses to *Candida* species.

STAR★METHODS

Detailed methods are provided in the online version of this paper and include the following:

- KEY RESOURCES TABLE
- CONTACT FOR REAGENT AND RESOURCE SHARING
- EXPERIMENTAL MODEL AND SUBJECT DETAILS
  - Fungal Culture
  - Clinical Strain Identification
- METHOD DETAILS
  - Flow Cytometry
  - dSTORM Sample Preparation
  - dSTORM imaging
  - Super-resolution data fitting
  - Super-resolution cluster analysis
  - Alcian Blue binding analysis
  - GPC analysis
  - NMR analysis
- QUANTIFICATION AND STATISTICAL ANALYSIS
- DATA AND SOFTWARE AVAILABILITY

SUPPLEMENTAL INFORMATION

Supplemental Information includes five figures and can be found with this article online at https://doi.org/10.1016/j.celrep.2018.07.088.

ACKNOWLEDGMENTS

We appreciate and acknowledge Janet Oliver for helpful scientific discussion and review of the manuscript as well as the members of the Neumann laboratory. We thank Dr. Karissa Culbreath and Christen Griego-Fullbright for their assistance with providing clinical isolate strains. This research was supported by the University of New Mexico Center for Spatiotemporal Modeling of Cell Signaling (STMC; NIH P50GM085273 [A.K.N. and K.A.L.] and R01AI116894 [A.K.N.]). M.S.G. was supported by fellowships from the STMC and an NIH T32 training grant (NIH T32 AI007538) during the course of this work. This work was also supported in part by Quillen College of Medicine, East Tennessee State University, through NIH grants GMR01053522 (D.L.W.), GMR01119197 (D.L.W.), GMR01083016 (D.L.W.), R15AI109581 (M.D.K.), and C06RR030651.

AUTHOR CONTRIBUTIONS

M.S.G. and A.K.N. conceived and designed experiments. M.S.G., M.D.K., D.L.W., D.W.L., C.M.M., and J.M.Y. performed the experiments. M.S.G., A.K.N., M.J.W., K.A.L., D.L.W., D.W.L., C.M.M., and H.C.P. analyzed data. M.J.W. contributed reagents, materials, and analysis tools. M.S.G., A.K.N., and M.J.W. wrote the manuscript.

DECLARATION OF INTERESTS

D.W.L. is an employee of AppRidge International, a company that was paid to perform mannan structural analysis as a part of this study. The remaining authors declare no competing interests.

Received: November 14, 2017
Revised: July 5, 2018
Accepted: July 27, 2018
Published: August 28, 2018

REFERENCES

Amarsaikhan, N., Sands, E.M., Shah, A., Abdolrasouli, A., Reed, A., Slaven, J.E., Armstrong-James, D., and Templeton, S.P. (2017). Caspofungin increases fungal chitin and eosinophil and γδ T cell-dependent pathology in invasive Aspergillosis. J. Immunol. *199*, 624–632.

Bugarcic, A., Hitchens, K., Beckhouse, A.G., Wells, C.A., Ashman, R.B., and Blanchard, H. (2008). Human and mouse macrophage-inducible C-type lectin (Mincle) bind Candida albicans. Glycobiology *18*, 679–685.

Chattaway, F.W., Holmes, M.R., and Barlow, A.J. (1968). Cell wall composition of the mycelial and blastospore forms of Candida albicans. J. Gen. Microbiol. *51*, 367–376.

Cutler, J.E. (2001). N-glycosylation of yeast, with emphasis on Candida albicans. Med. Mycol. *39* (*Suppl 1*), 75–86.

Davis, S.E., Hopke, A., Minkin, S.C., Jr., Montedonico, A.E., Wheeler, R.T., and Reynolds, T.B. (2014). Masking of β(1-3)-glucan in the cell wall of Candida albicans from detection by innate immune cells depends on phosphatidylserine. Infect. Immun. *82*, 4405–4413.

de Groot, P.W.J., Kraneveld, E.A., Yin, Q.Y., Dekker, H.L., Gross, U., Crielaard, W., de Koster, C.G., Bader, O., Klis, F.M., and Weig, M. (2008). The cell wall of the human pathogen Candida glabrata: differential incorporation of novel adhesin-like wall proteins. Eukaryot. Cell *7*, 1951–1964.

Elieh Ali Komi, D., Sharma, L., and Dela Cruz, C.S. (2018). Chitin and its effects on inflammatory and immune responses. Clin. Rev. Allergy Immunol. *54*, 213–223.

Ester, M., Kriegel, H., Sander, J., and Xu, X. (1996). A density based algorithm for discovering cluster in large spatial databases with noise. In Proceedings of the Second International Conference on Knowledge Discovery and Data Mining, E. Simoudis, J. Han, and U. Fayyad, eds. (AAAI Press), pp. 226–231.

Galán-Díez, M., Arana, D.M., Serrano-Gómez, D., Kremer, L., Casasnovas, J.M., Ortega, M., Cuesta-Domínguez, A., Corbí, A.L., Pla, J., and Fernández-Ruiz, E. (2010). Candida albicans beta-glucan exposure is controlled by the fungal CEK1-mediated mitogen-activated protein kinase pathway that modulates immune responses triggered through dectin-1. Infect. Immun. *78*, 1426–1436.

Gantner, B.N., Simmons, R.M., and Underhill, D.M. (2005). Dectin-1 mediates macrophage recognition of Candida albicans yeast but not filaments. EMBO J. *24*, 1277–1286.

Goodridge, H.S., Reyes, C.N., Becker, C.A., Katsumoto, T.R., Ma, J., Wolf, A.J., Bose, N., Chan, A.S.H., Magee, A.S., Danielson, M.E., et al. (2011). Activation of the innate immune receptor Dectin-1 upon formation of a 'phagocytic synapse'. Nature *472*, 471–475.

Gow, N.A., and Hube, B. (2012). Importance of the Candida albicans cell wall during commensalism and infection. Curr. Opin. Microbiol. *15*, 406–412.

Gow, N.A.R., Netea, M.G., Munro, C.A., Ferwerda, G., Bates, S., Mora-Montes, H.M., Walker, L., Jansen, T., Jacobs, L., Tsoni, V., et al. (2007). Immune recognition of Candida albicans β-glucan by dectin-1. J. Infect. Dis. *196*, 1565–1571.

Gow, N.A.R., van de Veerdonk, F.L., Brown, A.J.P., and Netea, M.G. (2011). Candida albicans morphogenesis and host defence: discriminating invasion from colonization. Nat. Rev. Microbiol. *10*, 112–122.

Graus, M.S., Pehlke, C., Wester, M.J., Davidson, L.B., Steinberg, S.L., and Neumann, A.K. (2014). A new tool to quantify receptor recruitment to cell contact sites during host-pathogen interaction. PLoS Comput. Biol. *10*, e1003639.

Hall, R.A., and Gow, N.A. (2013). Mannosylation in Candida albicans: role in cell wall function and immune recognition. Mol. Microbiol. *90*, 1147–1161.

Hall, R.A., Bates, S., Lenardon, M.D., Maccallum, D.M., Wagener, J., Lowman, D.W., Kruppa, M.D., Williams, D.L., Odds, F.C., Brown, A.J.P., and Gow, N.A. (2013). The Mnn2 mannosyltransferase family modulates mannoprotein fibril length, immune recognition and virulence of Candida albicans. PLoS Pathog. *9*, e1003276.

Hardison, S.E., and Brown, G.D. (2012). C-type lectin receptors orchestrate antifungal immunity. Nat. Immunol. *13*, 817–822.

Herrero, A.B., Magnelli, P., Mansour, M.K., Levitz, S.M., Bussey, H., and Abeijon, C. (2004). KRE5 gene null mutant strains of Candida albicans are avirulent and have altered cell wall composition and hypha formation properties. Eukaryot. Cell *3*, 1423–1432.

Hobson, R.P., Munro, C.A., Bates, S., MacCallum, D.M., Cutler, J.E., Heinsbroek, S.E., Brown, G.D., Odds, F.C., and Gow, N.A. (2004). Loss of cell wall mannosylphosphate in Candida albicans does not influence macrophage recognition. J. Biol. Chem. *279*, 39628–39635.

Hopke, A., Nicke, N., Hidu, E.E., Degani, G., Popolo, L., and Wheeler, R.T. (2016). Neutrophil attack triggers extracellular trap-dependent candida cell wall remodeling and altered immune recognition. PLoS Pathog. *12*, e1005644.

Inoue, M., and Shinohara, M.L. (2014). Clustering of pattern recognition receptors for fungal detection. PLoS Pathog. *10*, e1003873.

Itano, M.S., Steinhauer, C., Schmied, J.J., Forthmann, C., Liu, P., Neumann, A.K., Thompson, N.L., Tinnefeld, P., and Jacobson, K. (2012). Super-resolution imaging of C-type lectin and influenza hemagglutinin nanodomains on plasma membranes using blink microscopy. Biophys. J. *102*, 1534–1542.

Kasper, L., Seider, K., Gerwien, F., Allert, S., Brunke, S., Schwarzmüller, T., Ames, L., Zubiria-Barrera, C., Mansour, M.K., Becken, U., et al. (2014). Identification of Candida glabrata genes involved in pH modulation and modification of the phagosomal environment in macrophages. PLoS ONE *9*, e96015.

Kasper, L., Seider, K., and Hube, B. (2015). Intracellular survival of Candida glabrata in macrophages: immune evasion and persistence. FEMS Yeast Res. *15*, fov042.

Kaur, R., Ma, B., and Cormack, B.P. (2007). A family of glycosylphosphatidylinositol-linked aspartyl proteases is required for virulence of Candida glabrata. Proc. Natl. Acad. Sci. USA *104*, 7628–7633.

Klis, F.M., de Groot, P., and Hellingwerf, K. (2001). Molecular organization of the cell wall of Candida albicans. Med. Mycol. *39* (*Suppl 1*), 1–8.

Kruppa, M., Greene, R.R., Noss, I., Lowman, D.W., and Williams, D.L. (2011). C. albicans increases cell wall mannoprotein, but not mannan, in response to blood, serum and cultivation at physiological temperature. Glycobiology *21*, 1173–1180.

Kwofie, F. (2015). Candida albicans hyphal mannan is structurally distinct from yeast mannan. PhD thesis (East Tennessee State University). http://dc.etsu.edu/etd/2555.

Levet, F., Hosy, E., Kechkar, A., Butler, C., Beghin, A., Choquet, D., and Sibarita, J.B. (2015). SR-Tesseler: a method to segment and quantify localization-based super-resolution microscopy data. Nat. Methods *12*, 1065–1071.

Li, D., Williams, D., Lowman, D., Monteiro, M.A., Tan, X., Kruppa, M., Fonzi, W., Roman, E., Pla, J., and Calderone, R. (2009). The Candida albicans histidine kinase Chk1p: signaling and cell wall mannan. Fungal Genet. Biol. *46*, 731–741.

Lin, J., Wester, M.J., Graus, M.S., Lidke, K.A., and Neumann, A.K. (2016). Nanoscopic cell-wall architecture of an immunogenic ligand in Candida albicans during antifungal drug treatment. Mol. Biol. Cell *27*, 1002–1014.

Lowman, D.W., Ensley, H.E., Greene, R.R., Knagge, K.J., Williams, D.L., and Kruppa, M.D. (2011). Mannan structural complexity is decreased when Candida albicans is cultivated in blood or serum at physiological temperature. Carbohydr. Res. *346*, 2752–2759.

McKenzie, C.G., Koser, U., Lewis, L.E., Bain, J.M., Mora-Montes, H.M., Barker, R.N., Gow, N.A., and Erwig, L.P. (2010). Contribution of Candida albicans cell wall components to recognition by and escape from murine macrophages. Infect. Immun. *78*, 1650–1658.

Medzhitov, R., and Janeway, C.A., Jr. (1997). Innate immunity: the virtues of a nonclonal system of recognition. Cell *91*, 295–298.

Mora-Montes, H.M., Netea, M.G., Ferwerda, G., Lenardon, M.D., Brown, G.D., Mistry, A.R., Kullberg, B.J., O'Callaghan, C.A., Sheth, C.C., Odds, F.C., et al. (2011). Recognition and blocking of innate immunity cells by Candida albicans chitin. Infect. Immun. *79*, 1961–1970.

Netea, M.G., Gow, N.A.R., Munro, C.A., Bates, S., Collins, C., Ferwerda, G., Hobson, R.P., Bertram, G., Hughes, H.B., Jansen, T., et al. (2006). Immune sensing of Candida albicans requires cooperative recognition of mannans and glucans by lectin and Toll-like receptors. J. Clin. Invest. *116*, 1642–1650.

Netea, M.G., Brown, G.D., Kullberg, B.J., and Gow, N.A. (2008). An integrated model of the recognition of Candida albicans by the innate immune system. Nat. Rev. Microbiol. *6*, 67–78.

Nguyen, T.H., Fleet, G.H., and Rogers, P.L. (1998). Composition of the cell walls of several yeast species. Appl. Microbiol. Biotechnol. *50*, 206–212.

Poulain, D., Tronchin, G., Dubremetz, J.F., and Biguet, J. (1978). Ultrastructure of the cell wall of Candida albicans blastospores: study of its constitutive layers by the use of a cytochemical technique revealing polysaccharides. Ann. Microbiol. (Paris) *129*, 141–153.

Rayner, J.C., and Munro, S. (1998). Identification of the MNN2 and MNN5 mannosyltransferases required for forming and extending the mannose branches of the outer chain mannans of Saccharomyces cerevisiae. J. Biol. Chem. *273*, 26836–26843.

Roetzer, A., Gratz, N., Kovarik, P., and Schüller, C. (2010). Autophagy supports Candida glabrata survival during phagocytosis. Cell. Microbiol. *12*, 199–216.

Rouabhia, M., Schaller, M., Corbucci, C., Vecchiarelli, A., Prill, S.K., Giasson, L., and Ernst, J.F. (2005). Virulence of the fungal pathogen Candida albicans requires the five isoforms of protein mannosyltransferases. Infect. Immun. *73*, 4571–4580.

Ruiz-Herrera, J., Elorza, M.V., Valentín, E., and Sentandreu, R. (2006). Molecular organization of the cell wall of Candida albicans and its relation to pathogenicity. FEMS Yeast Res. *6*, 14–29.

Seider, K., Brunke, S., Schild, L., Jablonowski, N., Wilson, D., Majer, O., Barz, D., Haas, A., Kuchler, K., Schaller, M., and Hube, B. (2011). The facultative intracellular pathogen Candida glabrata subverts macrophage cytokine production and phagolysosome maturation. J. Immunol. *187*, 3072–3086.

She, X., Calderone, R., Kruppa, M., Lowman, D., Williams, D., Zhang, L., Gao, Y., Khamooshi, K., Liu, W., and Li, D. (2016). Cell wall N-linked mannoprotein biosynthesis requires Goa1p, a putative regulator of mitochondrial complex I in Candida albicans. PLoS ONE *11*, e0147175.

Sherrington, S.L., Sorsby, E., Mahtey, N., Kumwenda, P., Lenardon, M.D., Brown, I., Ballou, E.R., MacCallum, D.M., and Hall, R.A. (2017). Adaptation

of Candida albicans to environmental pH induces cell wall remodelling and enhances innate immune recognition. PLoS Pathog. *13*, e1006403.

Shibata, N., Kobayashi, H., and Suzuki, S. (2012). Immunochemistry of pathogenic yeast, Candida species, focusing on mannan. Proc. Jpn. Acad., Ser. B, Phys. Biol. Sci. *88*, 250–265.

Smith, C.S., Joseph, N., Rieger, B., and Lidke, K.A. (2010). Fast, single-molecule localization that achieves theoretically minimum uncertainty. Nat. Methods *7*, 373–375.

Trinel, P.-A., Maes, E., Zanetta, J.-P., Delplace, F., Coddeville, B., Jouault, T., Strecker, G., and Poulain, D. (2002). Candida albicans phospholipomannan, a new member of the fungal mannose inositol phosphoceramide family. J. Biol. Chem. *277*, 37260–37271.

Ueno, K., Okawara, A., Yamagoe, S., Naka, T., Umeyama, T., Utena-Abe, Y., Tarumoto, N., Niimi, M., Ohno, H., Doe, M., et al. (2013). The mannan of Candida albicans lacking β-1,2-linked oligomannosides increases the production of inflammatory cytokines by dendritic cells. Med. Mycol. *51*, 385–395.

Wagener, J., MacCallum, D.M., Brown, G.D., and Gow, N.A. (2017). Candida albicans chitin increases arginase-1 activity in human macrophages, with an impact on macrophage antimicrobial functions. MBio *8*, e01820–e16.

Wells, C.A., Salvage-Jones, J.A., Li, X., Hitchens, K., Butcher, S., Murray, R.Z., Beckhouse, A.G., Lo, Y.L., Manzanero, S., Cobbold, C., et al. (2008). The macrophage-inducible C-type lectin, mincle, is an essential component of the innate immune response to Candida albicans. J. Immunol. *180*, 7404–7413.

West, L., Lowman, D.W., Mora-Montes, H.M., Grubb, S., Murdoch, C., Thornhill, M.H., Gow, N.A.R., Williams, D., and Haynes, K. (2013). Differential virulence of Candida glabrata glycosylation mutants. J. Biol. Chem. *288*, 22006–22018.

Wheeler, R.T., and Fink, G.R. (2006). A drug-sensitive genetic network masks fungi from the immune system. PLoS Pathog. *2*, e35.

Wheeler, R.T., Kombe, D., Agarwala, S.D., and Fink, G.R. (2008). Dynamic, morphotype-specific Candida albicans beta-glucan exposure during infection and drug treatment. PLoS Pathog. *4*, e1000227.

STAR★METHODS

KEY RESOURCES TABLE

REAGENT or RESOURCE	SOURCE	IDENTIFIER
Antibodies		
Goat anti-Human IgG (H+L) Cross-Adsorbed Secondary Antibody, Alexa Fluor 488	Invitrogen	A11013
Goat anti-Mouse IgG1 Cross-Adsorbed Secondary Antibody, Alexa Fluor 647	Invitrogen	A21240
anti-β-glucan IgM	Gift from Biothera Pharmaceuticals	clone BfDIV
Chemicals, Peptides, and Recombinant Proteins		
Fc-hDectin-1a	Invivogen	fc-hdec1a
Catalase	Sigma-Aldrich	C40
Glucose Oxidase	Sigma-Aldrich	G0543
Cysteamine	Sigma-Aldrich	M9768
Alcian Blue	Sigma-Aldrich	A5268
Experimental Models: Organisms/Strains		
C. albicans: SC5314	ATCC	MYA-2876
C. albicans: Ca*mnn2Δ*	Gift from Neil Gow	N/A
C. albicans: Ca*mnn2Δ/mnn26Δ*	Gift from Neil Gow	N/A
C. albicans: sextuple mutant	Gift from Neil Gow	N/A
C. glabrata: ATCC2001	ATCC	ATCC2001
C. glabrata: Cg*mnn2Δ*	Gift from Ken Haynes	N/A
C. glabrata: Cg*mnn11Δ*	Gift from Ken Haynes	N/A
C. glabrata: Cg*anp1Δ*	Gift from Ken Haynes	N/A
C. albicans: TRL035	Clinical Isolate	N/A
C. glabrata: TRL031	Clinical Isolate	N/A
Software and Algorithms		
Fit probe positions using maximum likelihood-based algorithm	Smith et al., 2010	single molecule localization
H-SET	This paper	https://stmc.health.unm.edu/tools-and-data/index.html
Voronoï	Voronoï tessellation-based segmentation	https://stmc.health.unm.edu/tools-and-data/index.html
Other		
C-Chip Bulldog Bio	Bulldog Bio	DHC-N01
Calcofluor White	Sigma-Aldrich	F3543
Wheat Germ Agglutinin, Alexa Fluor 647 conjugate	Invitrogen	W32466
Alexa Fluor 647-NHS-ester	Invitrogen	A20006
Zeba Desalting Columns, 7kDA MWCO	Thermo Scientific	89882

CONTACT FOR REAGENT AND RESOURCE SHARING

Further information and requests for resources and reagents should be directed to and will be fulfilled by the Lead Contact, Dr. Aaron Neumann (akneumann@salud.unm.edu).

EXPERIMENTAL MODEL AND SUBJECT DETAILS

Fungal Culture

C. albicans. *C. albicans* (SC5314, ATCC, #MYA-2876), TRL035, and mannosylation mutants Ca*mnn2Δ*, Ca*mnn2Δ/mnn26Δ*, and sextuple deletion mutants were grown in YPD broth in an orbital incubator at 30°C for 16 hours to reach exponential growth phase.

All strains were then centrifuged and washed in PBS. C*amnn2Δ*, C*amnn2Δ/mnn26Δ*, and sextuple deletion mutants were a gift from Dr. Neil Gow (Hall et al., 2013). Strain authenticity is based on provision directly from the repository or generating laboratory.

C. glabrata. *C. glabrata* (ATCC, #2001) and TRL031 were grown in YPD and mannosylation mutants C*gmnn2Δ,* C*gmnn11Δ,* and C*ganp1Δ* were grown in SD. His^- media in an orbital incubator at 30°C for 16 hours to reach exponential growth phase. All strains were then centrifuged and washed in PBS. C*gmnn2Δ,* C*gmnn11Δ,* and C*ganp1Δ* were a gift from Dr. Ken Haynes (West et al., 2013). Strain authenticity is based on provision directly from the repository or generating laboratory.

Clinical Strain Identification

TRL031 and TRL035 were grown on YPD agar plates for 48 hours at 30°C. Single colonies were transferred to Charles River (Newark, DE) on YPD slants. Both TRL031 and TRL035 were identified as *C. glabrata* and *C. albicans* respectively by FunITS at Charles River.

METHOD DETAILS

Flow Cytometry

All strains of yeasts were treated similarly. After the PBS wash described above, yeast were counted on a hemocytometer (C-Chip Bulldog Bio, DHC-N01) to attain $3.5x10^6$ yeast total for primary and secondary staining. All strains were stained with 30 μg/ml of Fc-hDectin-1a (Invivogen, fc-hdec1a) or 10 μg/ml of murine anti-β-glucan IgM (clone BfDIV, gift of Biothera Pharmaceuticals) for 30 min at 25°C. The IgM probe was used for flow cytometric glucan exposure screening in clinical isolates. The Fc-hDectin-1a probe was used for all other glucan exposure experiments, including dSTORM. Yeasts were then centrifuged and washed with PBS three times. The secondary stain used to identify the primary probes was either AlexaFluor 488 conjugated anti-human IgG antibody (Invitrogen, A11013) for hDectin-1a or AlexaFluor 647 conjugated anti-murine IgM antibody (Invitrogen, A21240) for anti-β-glucan IgM. The secondary stain was added to the primary stained yeasts at 4 μg/ml for 30 minutes at 25°C in the dark and then washed three times with PBS. Data were acquired using a BD LSRFortessa flow cytometer (BD Biosciences). All data presented were pooled from triplicate biological replicates of the samples.

For chitin labeling, after the PBS wash described in the fungal culture methods, yeast were counted on a hemocytometer (C-Chip Bulldog Bio, DHC-N01) to attain $1x10^7$ cells/mL for staining with calcofluor white (Sigma-Aldrich, F3543) or wheat germ agglutinin Alexa Fluor 647 conjugate (Invitrogen, W32466). Changes in chitin content of the cell wall were detectable by calcofluor white, while changes in chitin exposure at the outer cell wall surface were assessed by wheat germ agglutinin. Yeast were stained with 25 μg/mL of calcofluor white or 5 μg/mL of wheat germ agglutinin for 10 minutes at 25°C in the dark, then centrifuged and washed in PBS three times. Data were collected using BD LSRFortessa flow cytometer (BD Biosciences). All data presented represents a triplicate of biological replicates.

dSTORM Sample Preparation

All yeasts strains prior to probe application were fixed with 4% PFA at room temperature for 15 minutes followed by extensive washing. Yeasts were then counted in a similar manner as samples prepared for flow cytometry. AlexaFluor 647 (Invitrogen, A20006) was used to label the soluble Fc-hDectin-1a. AlexaFluor 647-NHS-ester and Fc-hDectin-1a were mixed at 10:1 molar ratio in PBS at pH 8 for 1 hour at 25°C in the dark. To purify the labeled proteins, Zeba Desalting Columns (Thermo Scientific, 7-kDA MWCO, 89882) were used. Degree of labeling was found to be 1:1 molar ratio determined by absorption spectroscopy. Yeasts were then stained with the AlexaFluor 647 conjugated Fc-hDectin-1a at 30 μg/ml for 30 min at 25°C in the dark and then washed three times in PBS. Prior to imaging, the fixed/labeled samples were embedded in 1% agar on the coverslip to minimize motion during image acquisition.

While we acknowledge the limitations of performing experiments on non-viable cells, yeast fixation was necessary to: 1) mitigate possible mobility of cell wall moieties that would degrade dSTORM resolution and 2) to avoid complications to data interpretation inherent in potential fungal cell wall responses to the imaging conditions necessary for dSTORM imaging. Furthermore, our observations indicate that PFA fixation alone does not an induce artifactual increase in glucan exposure on yeast (data not shown).

dSTORM imaging

Imaging methods were duplicated from Lin et al. (Lin et al., 2016). In summary, the agar embedded samples had an imaging buffer applied to them for 15 minutes prior to imaging. Imaging buffer contained 50mM Tris, 10% (wt/vol) glucose, 10 mM NaCl, 40 μg/ml catalase (Sigma-Aldrich, C40), 500 μg/ml glucose oxidase (Sigma-Aldrich, G0543), and 10 mM cysteamine (Sigma-Aldrich, M9768), pH 8. Data acquisition was on an Olympus IX-71 microscope equipped with an objective-based TIRF illuminator using an oil-immersion objective (PlanApo N, 150 × /1.45 NA; Olympus) in an oblique illumination configuration. Sample excitation was done with a 637nm laser (Thorlabs, laser diode HL63133DG), with custom-built collimation optics. To ensure that minimal drift occurred during data acquisition, a self-registration algorithm was implemented.

Super-resolution data fitting

To fit probe positions from raw dSTORM data, we used a maximum likelihood-based algorithm from Smith et al. (Smith et al., 2010). Our positional fitting parameters included: normal fitting with a Cramer-Rao lower bound (CRLB) based fit precision threshold of

0.2 pixels or 22 nm. This suppressed the contribution of positionally inaccurate fits arising from rare events where multiple dyes were emitting simultaneously in a diffraction-limited volume. Fluorophores identified in time frames with a frame gap of one to four frames were combined into a single, improved fit when the spatial proximity passed a hypothesis test with 0.05 level of significance. Frame connection suppressed overrepresentation of fits from dyes with unusually long on-times, which is expected from the exponential distribution of dye on-times.

Super-resolution cluster analysis

Analysis of nanostructure in our dSTORM datasets proceeded in three steps: estimating the positions of single emitter probes, identifying spatial clusters of exposed glucan labeled by probes, and quantifying feature characteristics thus identified.

Hierarchical Single Emitter Hypothesis Test

Single probes can be observed more than once, with positional error, in dSTORM datasets. This contributes some overestimation of probe density and feature size. The purpose of the Hierarchical Single Emitter Hypothesis Test (H-SET) algorithm is to estimate the positions of single emitter probes and minimize such errors in subsequent cluster identification steps.

All image data was run through pass 1 of H-SET, a top-down hierarchical clustering algorithm implemented in MATLAB that collapses clusters of observations of blinking fluorophores into single estimates of the true locations (localizations) of the fluorophores (Lin et al., 2016). Essentially all collapses occur in pass 1, which requires only one user specified parameter, a level of significance for the hypothesis test (LoS = 0.01 was used), to make its decisions.

Pass 2 of H-SET determines clustering of exposures by using some known clustering algorithm, which for distance or density based methods (e.g., hierarchical or DBSCAN (Ester et al., 1996)) typically depends on two parameters: a distance metric, epsilon, the maximal distance between two points within a cluster, and the minimal number of points (minPts) required to form a cluster. These parameters define the type of cluster that will be detected, and it is often impossible to know these values *a priori* for biological structures. We optimized the choice of epsilon and minPts in a data driven fashion.

At any given parameterization of epsilon and minPts, spurious clusters can be detected in a spatially random distribution of points once the density of points becomes high enough. We sought to parameterize epsilon and minPts such that detection of spurious clustering in simulated random distributions would be minimized, while still remaining sensitive enough to detect clusters in datasets. Therefore, we optimized epsilon and minPts using the mean density of localizations in our densest datasets, which was 649 localizations per ROI for the *C. albicans* sextuple mutant dataset (eight ROIs over five images).

To determine values for epsilon and minPts, H-SET pass 2 hierarchical clustering (MATLAB linkage function) was performed on the sextuple mutant dataset for a range of epsilons and minPts (20-40 nm by 1 nm and 5-15, respectively), computing the number of multiglucan exposure sites, N_{multi}, for each combination averaged over all the ROIs. These values were compared with the mean results from n = 25 random simulations generated over the same ranges of epsilon and minPts, the simulated localizations being distributed uniformly and randomly over the ROI, and the number of which were computed from a Poisson distribution with mean based on the average number of localizations determined from the sextuple mutant data. The biggest difference between N_{multi} for the two datasets, remaining sensitive to detection of multiglucan exposure sites for the experimental data but minimizing their spurious detection for the random simulated data, produced unique values for epsilon and minPts: 20 nm and 6, respectively, for *C. albicans*, and 26 nm and 5, respectively, for *C. glabrata*. Figure S5 shows 3D plots of N_{multi} as a function of epsilon and minPts for the two datasets, (Figure S5A) experimental and (Figure S5B) random simulated, as well as their difference (Figure S5C).

Voronoï tessellation-based segmentation

To verify that the trends observed were independent of the clustering algorithm employed, the analyses were recomputed using the Voronoï-based algorithm of Levet et al. (Levet et al., 2015), using our own MATLAB implementation. The algorithm proceeds by constructing a Voronoï diagram of image points (Figure S6A, localizations). A Voronoï diagram is a partitioning of a region based on a set of seeds (points) within that region such that any location in a given cell is closer to the seed used to generate that cell than the seeds used to form the other cells. See Figures S5D and S5E. Polygon P_i^0 corresponds to seed (point) S_i and has area A_i^0. First rank neighbors are those polygons P_{ij}^1 sharing edges with P_i^0, which when combined together with P_i^0 form the rank 1 polygon P_i^1. The rank 1 area A_i^1 is then the sum of the areas $\sum_j A_{ij}^1 + A_i^0$. From these, densities δ^k (k is the rank) can be computed by dividing the number of points in P_i^k by A_i^k. For further clarification, see Levet et al., Figure 1 (Levet et al., 2015).

At this point, object segmentation (clustering) is initiated. For example, if δ is the average density of the data distribution, then clustering proceeds by merging all rank k polygons that satisfy

$$\delta_i^1 \geq \alpha\delta$$

where $\alpha > 0$ (k = 1 and $\alpha = 2$ are typical choices in Levet et al.'s analyses).

The polygons satisfying the above criterion that are adjacent to each other form potential clusters of the seeds that generated them, and are merged into single clusters if the final collections have the user specified minimum number of points, minPts. Figure S6B displays the clustering results based on the partitioning shown in Figure S6A, which was based on one ROI of the sextuple mutant dataset.

Similar to what was done previously, pass 2 H-SET was performed using the Voronoï based algorithm with k = 1 over ranges of α (1-3 by increments of 0.25) and minPts (3-15), computing once again the number of multiglucan exposure sites. These were

compared, as before, with random simulated results, choosing values for α and minPts where the difference between the experimental data and the random simulated results was the greatest at an α and minPts: 2 and 5 respectively for *C. albicans* and 2 and 4, respectively, for *C. glabrata*.

Alcian Blue binding analysis

Alcian Blue binding assay was adapted from Hobson et al. (Hobson et al., 2004). Yeasts were grown for 16 hours, washed, counted to achieve a number of $1x10^7$ cells/ml and suspended in 25 μg/ml of Alcian Blue (Sigma Aldrich, A5268) in 0.02 M HCl for 25 minutes at room temperature before being centrifuged and pelleted. Supernatant was then measured in a plate reader at A_{600}. Alcian Blue concentrations were calculated against a standard curve. Alcian Blue binding (x A_{600} units/cell) was found by calculating the initial A_{600} (u), the final A_{600} (v), and (n) the number of cells stained. These values were input into the formula: $x = (u - v) / n$. Data is presented as normalized to the mean of type strain Alcian Blue binding. All data presented was pooled from triplicate biological replicates of the samples.

GPC analysis

Cultivation of fungal strains

C. albicans strains were grown overnight (16hr) in 2L of YPD (2% Dextrose, 2% Peptone, 1% Yeast Extract). The cells were harvested by centrifugation at 5000 x g and stored at −20°C until they were needed for mannan extraction.

Isolation of cell wall mannan by mild alkali bath

Mannans were isolated using a method (Kwofie, 2015) that utilized a mild alkali extraction with boiling for 20 min. The extracted samples were harvested by centrifugation and neutralized. The neutralized material then was split in two and one-half treated with 50 mg/sample pronase (heat treated 25 min at 65°C to remove glycosidic activity) for 18 hours at 37°C in order to reduce the protein component of the mannoprotein. All samples were subjected to carbohydrate precipitation by addition of four volumes of methanol and samples were allowed to sit while the material settled. Once the material had settled, the supernatant was decanted and the remaining methanol blown off by blowing air over the sample. The dried sample was then resuspended in dH_2O, frozen, lyophilized and stored at −20°C until it was analyzed.

Gel permeation chromatographic analysis of C. albicans cell wall mannan/mannoprotein

The molecular weight, polydispersity, polymer distribution and Mark-Houwink (α) values were derived from gel permeation chromatography (GPC) with a Viscotek/Malvern GPC system consisting of a GPCMax autoinjector fitted to a TDA 305 detector (Viscotek/Malvern, Houston, TX). The TDA contains a refractive index detector, a low angle laser light scattering detector, a right angle laser light scattering detector, an intrinsic viscosity detector and a UV detector (λ = 254 nm). Three Waters Ultrahydrogel columns, i.e, 1200, 500 and 120, were fitted in series (Waters Corp. Milford, MA). The columns and detectors were maintained at 40°C within the TDA 305. The system was calibrated using Malvern pullulan and dextran standards. The mobile phase was 50mM sodium nitrite. The mobile phase was filter sterilized (0.45 μm into a 5 L mobile phase reservoir). Mannan samples were dissolved (3 mg/ml) in mobile phase (50 mM sodium nitrite, pH 7.3). The samples were incubated for ~60 min at 60°C, followed by sterile filtration (0.2 μm) and injected into the GPC (200 μL). Sample recovery was routinely > 98%. The data were analyzed using Viscotek OmniSec software v. 4.7.0.406. dn/dc was calculated using the OmniSec software (v. 4.6.1.354). dn/dc for the mannan samples was determined to be 0.145. The data were analyzed using a single peak assignment in order to obtain an average Mw for the entire polymer distribution. Replicate analysis of calibration standards indicated reproducibility of + or - 3%, which is well within the limits of the technique.

NMR analysis

NMR data acquisition and analysis is based on methods from Lowman et al. (Lowman et al., 2011). In summary, ^1H NMR spectra for mannan were collected on a Bruker Avance III 600 NMR spectrometer using a DCH cryoprobe operating at 345°K (72°C) in 5mm NMR tubes as reported previously(Lowman et al., 2011). Mannan (about 10 mg) was dissolved in about 600 μL DH_2O (Cambridge Isotope Laboratories, 99.8+% deuterated). Chemical shift referencing was accomplished relative to TMSP at 0.0 ppm. NMR spectra were collected and processed as follows: 256 scans, 2 pre-scans, 32,768 data points, 20 ppm sweep width centered at 6.2 ppm, and 1 s pulse delay. Spectra were processed using exponential apodization with 0.3 Hz line broadening and the JEOL DELTA software package (version 5.0.4.4) on a MacBook Pro (operating system OSX Yosemite 10.10.5). COSY spectra were collected as 2048 by 256, processed as 1024 by 1024, 8 pre-scans, 16 scans, sweep width 9 ppm centered at 4.7 ppm, and relaxation delay 1.49 s. Processing was accomplished with sine apodization in both dimensions using TopSpin (version 3.5 pl 3) on the MacBook Pro.

QUANTIFICATION AND STATISTICAL ANALYSIS

Bar graphs were used to display the median of the integrated intensity of β-glucan on the yeast cells as measured by flow cytometry. Error bars represent the standard deviation of the data. Student's t test, single-tail was used to determine statistical significance. Boxplots were used to display population distributions for dSTORM datasets. These plots depict a median (solid line) within a box representing the interquartile range (25th to 75th percentile of the population). The whiskers below and above the box represent the 1st and 99th percentiles of the dataset. Crosses are used to depict data points that fell outside of the whiskers. Mann-Whitney U test was used to determine statistical significance of the boxplots and was implemented by MATLAB functions.

Specific statistical tests, values of "n" replicates, the nature of the replicates and statistical significance values are found in the Figure legends.

DATA AND SOFTWARE AVAILABILITY

Computer code. Software used for data analysis and simulation is accessible at https://stmc.health.unm.edu/tools-and-data/index.html, including Image Analysis Tools and MATLAB Clustering Classes.